Electronic Supplementary Material (ESI) for Journal of Materials Chemistry A.

Supplementary information

Li^+ Storage and Transport in High-Voltage Spinel-$LiNi_{0.5}Mn_{1.5}O_4$ Codoped with F^- and Cu^{2+}

Dae-wook Kim[a,‡] , Hiromasa Shiiba[a,‡], Katsuya Teshima* [a, b] , and Nobuyuki Zettsu* [a, b, c]

a Department of Materials Chemistry, Faculty of Engineering, Shinshu University, 4-17-1 Wakasato, Nagano 380-8553, Japan

b Research Initiative for Supra-Materials, Shinshu University, 4-17-1 Wakasato, Nagano 380-8553, Japan

c Energy Landscape Architectonics Brain Bank (ELab2), Shinshu University, 4-17-1 Wakasato, Nagano 380-8553, Japan

‡These authors contributed equally

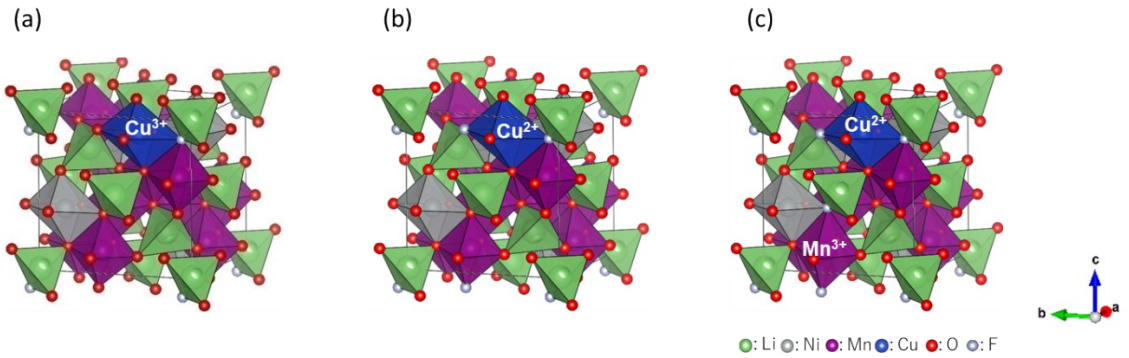

Figure S1. The DFT-calculated atomic arrangements of the most stable $LiNi_{0.5}Mn_{1.375}Cu_{0.125}O_{4-x}F_x$ in 56-atom supercell structures for (a) x = 0.125 (single F^- incorporation into the supercell, $Li_8Ni_4Mn_{11}Cu_1O_{31}F_1$), (b) x = 0.250 (double F^- incorporation, $Li_8Ni_4Mn_{11}Cu_1O_{30}F_2$), and (c) x = 0.375 (triple F^- incorporation, $Li_8Ni_4Mn_{11}Cu_1O_{29}F_3$). For x = 0.125, the F and Cu atoms preferably occupied O-sites (24e sites instead of the 8c sites) and Mn-sites (12d) irrespective of the number of incorporated F^-. Fluorine atom preferentially occupied 24e sites where it simultaneously coordinates Ni, Mn, and Cu ions. For x = 0.250, the second F atom per unit cell coordinates preferentially to Cu to form octahedral CuO_4F_2. It forms a trans $–F^-–Cu^{2+}–F–$ conformation along the b-axis. According to the ionic radius ratio rule, the formation energy of the *trans* conformation was lower than that of the *cis* form (by 0.13 eV). For x = 0.375, the incorporation of further F^- promoted the formation of octahedral MnO_4F_1 and favored the reduction of Mn^{4+} to Mn^{3+}. The XRD experiments indicated lattice parameter changes that occurred with increasing F^- substitution. The relatively small increase of the lattice parameter in highly fluorinated $LNMCOF_x$ may be from passivation of the oxygen deficiency by the F- at the defect site. Our calculations predicted a crystal structure transition from a cubic to orthorhombic system with F^- substitution, accompanied by an anisotropic lattice dilatation along the b-axis, whereas further F incorporation mitigated this dilatation, and it recovered to cubic system. This behavior was explained by the decrease of bond length along the b-axis caused by the formation of trans $–F^-–Cu^{2+}–F–$ conformation and the increase of bond length along the c-axis caused by the formation of Jahn-Teller distortion based on the $–F^-–Mn^{3+}–$ bond formation. In other words, it is concluded that the anisotropic Jahn - Teller distortion produced by Mn^{3+} is distributed in three directions of *a*, *b* and *c* axes by the dual substitution of Cu and F. For x = 0.375, the enhancement of anisotropic lattice dilatation along the c-axis was ascribed to the Jahn-Teller distortion of Mn^{3+} associated with the formation of trans $–F^–Mn^{3+}–F–$ conformation. We further calculated the Ni^{2+}/Mn^{4+} antisite defect formation energies for the LNMCOF*x* systems. The results were summarized below. The formation energy represented here showed positive value and was increased as the F^- substitution. These all results suggest that the symmetry transition was highly localized in a space near point of extrinsic defects Cu_{Mn} in the spinel framework. It is highly probable that randomization of the Ni^{2+}/Mn^{4+} is preferably occurred far from the Cu_{Mn} in association with the formation of Jahn-Teller Mn^{3+} distortion which is stabilized by the trans $–F^-–Cu^{2+}–F–$ conformation.

$LiNi_{0.5}Mn_{1.375}Cu_{0.125}O_4$	Ni/Mn antisite energy [eV]
①	-0.133
$LiNi_{0.5}Mn_{1.375}Cu_{0.125}O_{3.875}$	Ni/Mn antisite energy [eV]
①	0.120
$LiNi_{0.5}Mn_{1.375}Cu_{0.125}O_{3.875}F_{0.125}$	Ni/Mn antisite energy [eV]
①	0.115
$LiNi_{0.5}Mn_{1.375}Cu_{0.125}O_{3.75}F_{0.25}$	Ni/Mn antisite energy [eV]
①	0.320

	$LiNi_{0.5}Mn_{1.375}Cu_{0.125}O_{3.625}F_{0.375}$	Ni/Mn antisite energy [eV]
①	Cu-Ni@1F	0.303
②	Cu-Ni@0F	0.445
③	Ni@1F-Mn@1F_1	0.692
④	Ni@1F-Mn@1F_2	0.754
⑤	Ni@1F-Mn@2F	0.745
⑥	Ni@0F-Mn@2F	0.330

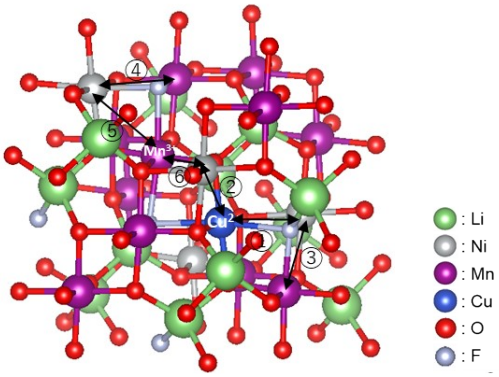

$LiNi_{0.5}Mn_{1.375}Cu_{0.125}O_{3.625}F_{0.375}$

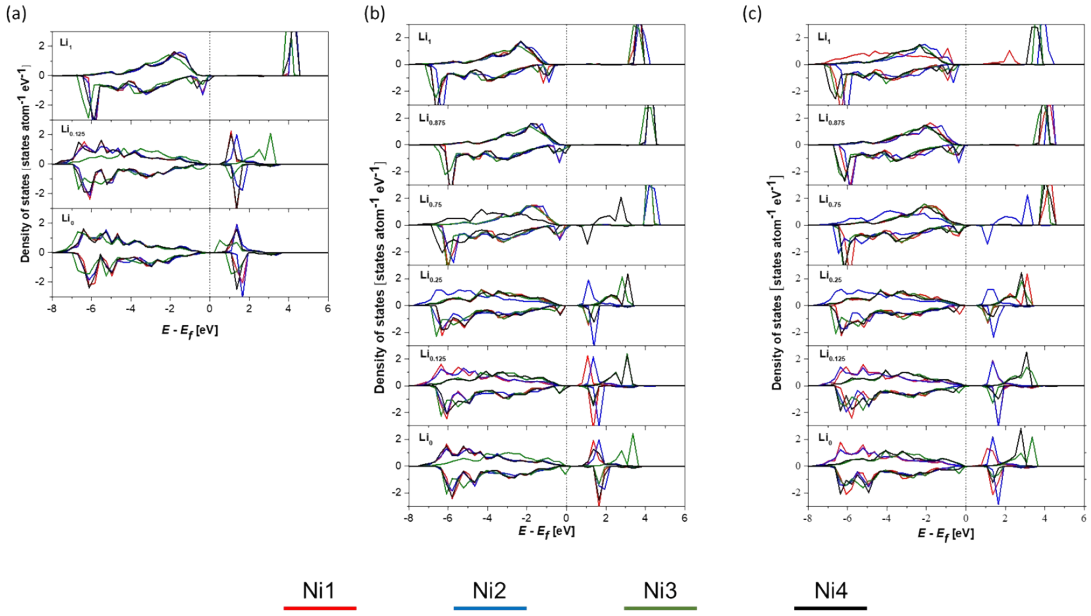

Figure S2. The DFT-calculated partial density of states (PDOS) for the Ni *3d* in LNMCOF$_x$ materials with various Li contents (a) x = 0.125, (b) x = 0.250, and (c) x = 0.375.

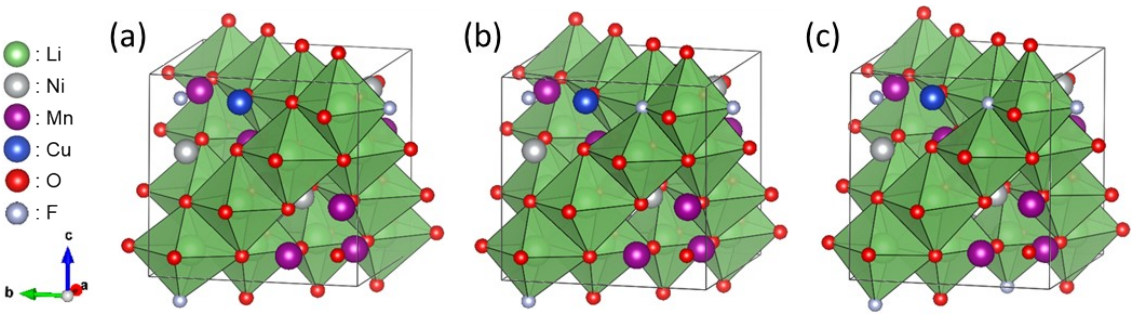

Figure S3. The DFT-calculated the most stable atomic configurations of $L_{1.125}NMCOF_x$ ($P4_332$ symmetry group) with various amounts of F^- per unit cell: (a) $x = 0.125$, (b) $x = 0.250$, and (c) $x = 0.375$. Extra Li^+ ions occupy empty octahedral sites in the spinel lattice

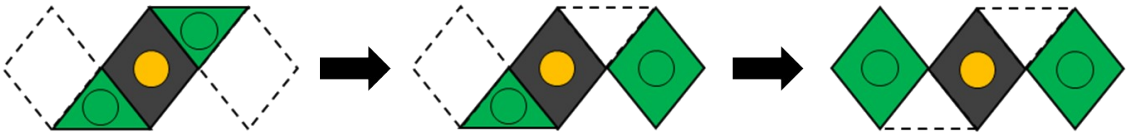

Figure S4. The plausible mechanism of extra Li^+ ion diffusion behavior conducted by the DFT-calculation: The Li^+ ions inserted into these sites are believed to promote the diffusion of nearest-neighbor Li^+ ions occupying tetrahedral sites to adjacent octahedral sites with relatively large volumes under the action of ionic repulsion.

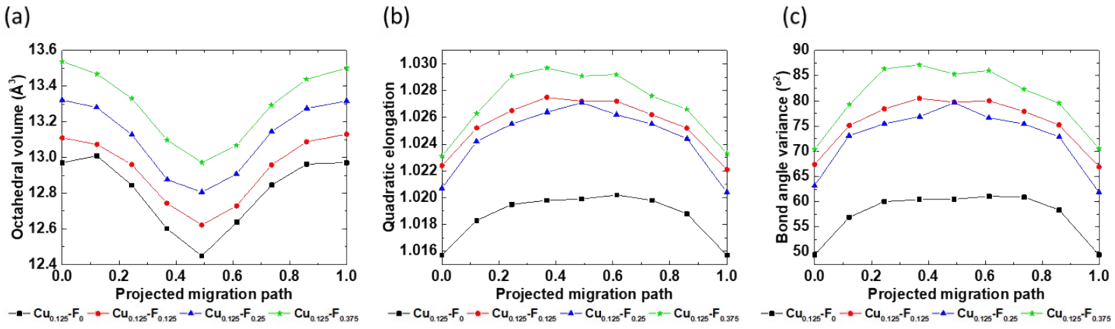

Figure S5. The calculated volume (a), quadratic elongation (b), and bond angle (c) variances for octahedral Li^+ vacancy sites in the Li^+ diffusion path of LNMCO and LNMCOF_x. The Li^+ vacancy site space volume in LNMCOF_x system became larger as F^- doping amount. Thus, F^- doping contributed to site volume expansion to facilitate the storage of excess Li^+.

Table S1. The chemical compositions of the LNMCOF$_x$ crystals, as evaluated by inductively coupled plasma optical emission spectrometry and X-ray photoelectron spectroscopy.

	Chemical composition
LNMO	$Li_{1.01}Ni_{0.49}Mn_{1.50}O_{4-\delta}$
LNMCO	$Li_{1.00}Ni_{0.49}Mn_{1.49}Cu_{0.01}O_{4-\delta}$
LNMCOF$_{0.03}$	$Li_{1.01}Ni_{0.49}Mn_{1.49}Cu_{0.01}O_{3.97}F_{0.03}$
LNMCOF$_{0.06}$	$Li_{0.99}Ni_{0.49}Mn_{1.49}Cu_{0.01}O_{3.94}F_{0.06}$
LNMCOF$_{0.12}$	$Li_{1.02}Ni_{0.49}Mn_{1.49}Cu_{0.01}O_{3.88}F_{0.12}$

Table S2. The contribution of Mn^{3+}/Mn^{4+} redox pair to specific capacity on the discharge curves

	[a]Mn^{3+} (%)
$LiNi_{0.5}Mn_{1.50}O_4$	2.33
$LiNi_{0.5}Mn_{1.49}Cu_{0.01}O_4$	2.62
$LiNi_{0.5}Mn_{1.45}Cu_{0.01}O_{4-x}F_{x/4}$	2.74
$LiNi_{0.5}Mn_{1.49}Cu_{0.01}O_{4-x/2}F_{x/2}$	4.03
$LiNi_{0.5}Mn_{1.49}Cu_{0.01}O_{4-x}F_x$	8.41

[a]calculated from capacity contribution at 4 V plateau

Table S3. The DFT-calculated the average oxidation state of $LNMCOF_x$ crystals in response to delithiation process.

	Z	0	0.125	0.25	0.75	0.875	1
x= 0.125	Ni	+2	-	-	-	+3.75	+4
	Mn	+4	-	-	-	+4	+4
	Cu	+3	-	-	-	+3	+2
x= 0.25	Ni	+2	+2	+2.25	+3.25	+3.5	+3.75
	Mn	+4	+4	+4	+4	+4	+4
	Cu	+2	+3	+3	+3	+3	+3
x= 0.375	Ni	+2	+2	+2.25	+3.25	+3.5	+3.5
	Mn	+3.91	+3.91	+3.91	+3.91	+3.91	+4
	Cu	+2	+3	+3	+3	+3	+3

Table S4. Impedance parameters for the LNMO and $LNMCOF_x$ crystal-based cathode/Li cells.

	D_{Li} (cm^2s^{-1})	R_{ct} (Ω)	R_{sf} (Ω)
Initial			
LNMO	$3.45x10^{-12}$	34.24	19.08
LNMCO	$7.83x10^{-12}$	13.87	23.47
$LNMCOF_{0.03}$	$9.24x10^{-12}$	9.98	19.44
$LNMCOF_{0.06}$	$1.12x10^{-11}$	9.81	18.75
$LNMCOF_{0.12}$	$7.46x10^{-11}$	9.78	19.76
After 200 cycles			
LNMO	$9.95x10^{-13}$	96.31	32.88
LNMCO	$4.85x10^{-12}$	20.24	30.23
$LNMCOF_{0.03}$	$5.41x10^{-12}$	12.16	24.76
$LNMCOF_{0.06}$	$8.59x10^{-12}$	11.39	23.87
$LNMCOF_{0.12}$	$5.39x10^{-11}$	11.21	21.76